A 3-D Visualization Method for Image-Guided Brain Surgery

N. G. Bourbakis, *Fellow, IEEE* and M. Awad

***Abstract*—This paper deals with a three-dimensional (3-D) methodology for brain tumor image-guided surgery. The methodology is based on development of a visualization process that mimics the human surgeon behavior and decision-making. In particular, it originally constructs a 3-D representation of a tumor by using the segmented version of the two-dimensional (2-D) MRI images. Then it develops an optimal path for the tumor extraction based on minimizing the surgical effort and penetration area. A cost function, incorporated in this process, minimizes the damage surrounding healthy tissues taking into consideration the constraints of a new snake-like surgical tool proposed here. The tumor extraction method presented in this paper is compared with the ordinary method used on brain surgery, which is based on a straight-line based surgical tool. Illustrative examples based on real simulations present the advantages of the 3-D methodology proposed here.**

***Index Terms*—Imaging, MRI guided brain surger, three-dimensional (3-D) visualization.**

I. Introduction

UNTIL recent decades, morbidity and unsuccessful surgeries were accepted by both the surgical society and the patients as unavoidable consequences of therapy. In traditional neuro-surgery, visualization is incomplete. The surgeon, relying on the small surgical opening lacks the spatial clues to assess the tumor's extent and to plan the extraction in the least risky approach. With the recent advances in radiology, the available imaging modalities such as CT, PET, MRI, fMRI, and MRA contribute to the reduction in the mortality rates by providing insight for surgical planning and replacing the minimally invasive surgeries [1]–[10], [15]–[18], [20]. Two-dimensional (2–D) and localizing the tumor within the complex anatomical neighborhood of the brain cells is a challenging problem. Due to the new computer and communication technologies, coupled with the always improved resolution in imaging and display systems, several software tools, such as Brain Voyager, Voxeline, VoxBlast, Neuronavigator, Volpack, etc., have been developed and used for reconstructing 3-D views from the stack of preoperative 2-D images [19] and [21]. As a result surgical planning and decision making improved, cutting short the surgical time and allowing the surgeon to concentrate more on executing the preoperative plan than to decide subsequent steps. Moreover, nowadays available in selected centers, a new system called the intra-operative MRI coregisters the patient coordinates, the surgical tool, the preoperative images as well as images acquired during surgery allowing almost real time navigation and reducing to a minimum any potential misconception of the problem's extent. Depending on the tumor location inside the human brain, surgery is usually the first step in treating brain tumors. Due to state of the art imaging techniques and instrumentation, 90–99% surgical removal is now really possible with preservation of surrounding healthy brain [1], [2].

Diagnostic imaging techniques facilitate in localizing lesions and tumors as well as determine the topographical relations between the lesions and the anatomic intracranial structures. Diagnostic accuracy allows the surgeon to work precisely with an increasing efficiency. Smaller incisions, less tissue trauma, and better surgical planning have reduced the risk of brain surgery from almost 90% in the 1940s to about 2% in the 1990s [2], [25].

However, due to the special set up in the operating room that creates a magnetic field of 0.5 T, no robotic devices can be used and the operation ends up being "decided" and executed by human surgeons. But what if the surgeon has a pronounced hand tremor, or lacks some expert' techniques? The operation outcome could be severely jeopardized and despite all the state of the art 3-D visualization, instrumentation and coregistration techniques, the surgery would be closer to a traditional case in that success is greatly affected by luck. Today, all the MRI driven brain surgeries use the same surgical tool and more or less the same approach, "a straight line-based penetration of the brain" by the surgical tool for extracting a candidate tumor [4], [10], [27].

In this paper, we propose a different visualization process that mimics the surgeon decision making. Taking into consideration surgical expertise' practices as well as surgical tool constraints, the algorithm would analyze every case and return the optimal path that can be executed by a surgeon or by a flexible robotic arm using a new surgical tool "snake-like" presented here.

II. Traditional Surgery

Visualization during traditional surgery is an inherent problem. Because of the small surgical opening and the reduction of light intensity in the depth of the operating field, the surgeon lacks the spatial clues to accurately understand the tumor extent and its localization with respect to vital cells: he or she cannot see beyond the exposed surface. The whole surgery depends on hand and eye coordination and often results in nonoptimal surgical approaches specially for reaching deep tumors where incision of healthy cells is expensive in terms of patient's safety and recovery rate.

Manuscript received May 17, 2001; revised January 22, 2003. This paper was recommended by Associate Editor K. Pattipati.

N. Bourbakis is with the Information Technology Research Institute, College of Engineering and Computer Science,Wright State University, Dayton, OH 45435-001 (e-mail bourbaki@cs.wright.edu).

M. Awad is with the AIIS Inc., Binghamton, NY.

Digital Object Identifier 10.1109/TSMCB.2003.816926

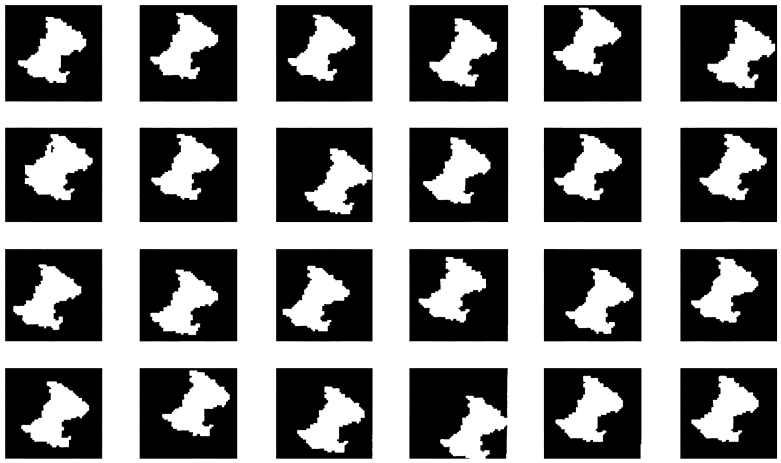

Fig. 1. Tumor shape extraction from 2-D MRI images.

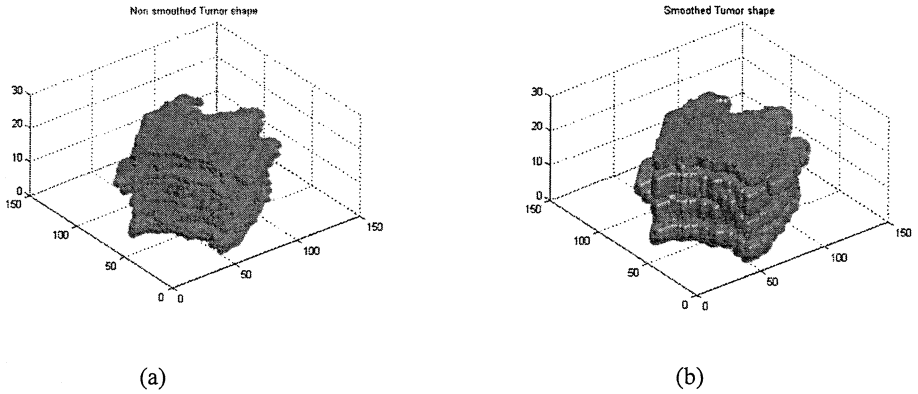

Fig. 2. Enhanced MRI set.

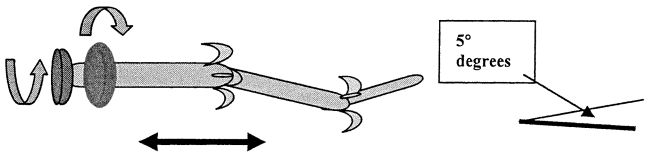

Fig. 3. Vertical cross section of the surgical tool.

TABLE I
N represents the slice number and θ is for degrees.

N	4	7	10	13
ϑ^0	5	4	2.5	1.5

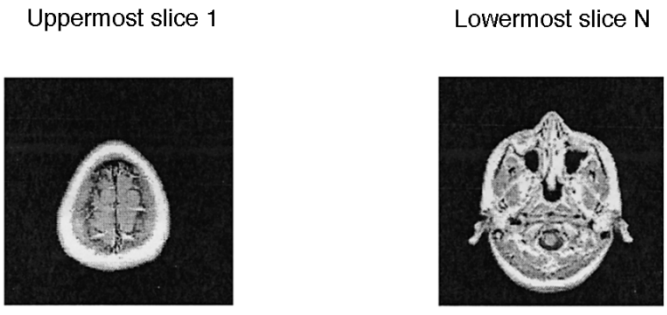

Fig. 4. Uppermost and lowermost slices.

A. Intra-Operative MRI [11]

Recent advances in imaging techniques, acquisition equipment, visualization software tools are making medicine improve at quick pace into image guided surgery. Now, the hand of the surgeon can be guided in mid-operation. Localization of tumors or lesions, assessments of their extents, as well as an optimal safe path for tumor resection are being available in today's operating rooms. The latter development allows surgical manipulation under direct visualization of the brain contents through both the eyes of the surgeon and the volumetric images of the MRI system. During the actual surgery, the previously acquired fMRI, MRA, and MRI (under a 1.5 T field) are coregistered in a frameless stereotactic manner into the physical space of the patient together with the near real time images that are acquired during the course of the surgery. The use of LED based optical tracking of surgical instruments precisely localizes the surgical instrument end with respect to the anatomic structure of the MRI images [1].

In this way the surgeon is able to assess the progress in the surgery and to modify, if need be, his or her preplanned approach during the surgery. The surgeon can account for instance for the actual path of the surgical tool, for some patient's movement, and for brain shifting [28]. Brain shift is a major problem for a surgery not discussed here.

Fig. 5. Mid-points.

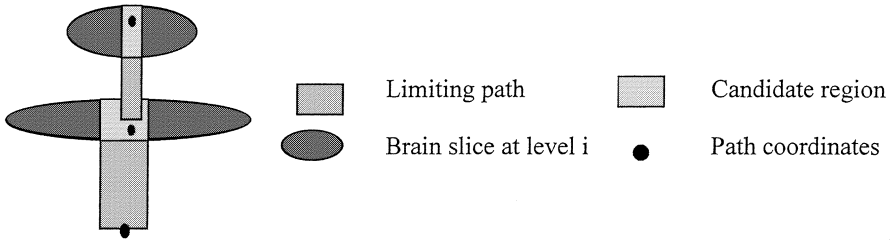

Fig. 6. Approach A.

III. 3-D Representation of Tumors

The 3-D representation of a tumor is based on the accurate extraction of the 2-D shape of the tumor from the corresponding MRI images [12]–[14], [22], [24], [26]. Thus, the extraction of the shape of a tumor, requires the 2-D MRI segmented images are to be searched for the particular value of the tumor. The pixels' positions of the tumor are stored and the marching cube algorithm is applied to get the 3-D surface representation. For simulation purposes, MRI slices were corrupted with tumor, the whole set of 27 MRI slices were searched, shape extraction using the edge detection technique at every level is applied and the region of interest is extracted. Tested and simulated results are shown in Figs. 1 and 2.

The 3-D tumor representation for this case is shown in Fig. 2(a). Applying a Gaussian filter the 3-D representation is smoothed, as shown in Fig. 2(b).

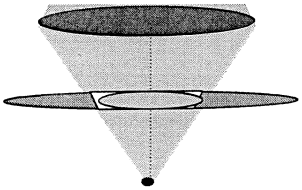

Fig. 7. Approach B.

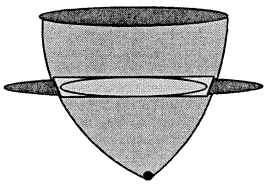

Fig. 8. Approach C.

IV. A Surgical Tool and an Optimal Path Approach for Tumors Extraction

A. Design of a New Flexible Surgical Tool [23]

The design and construction of any innovative device especially one dedicated for neurosurgery is always a great challenge for engineers. A successful design of a safe, useful design had to meet medical standards, surgeons and patients needs. Typically it is difficult to have a reliable and ready to use device in a one-shot development life cycle. Many prototypes are tested and their feedback reports provide guidance toward quicker and safer results. Although medical robotics is relatively a new technology for neuro-surgery, there is no dispute for having robotics replacing physical human process. Research is being focused on the instrumentation part for neuro-surgery both from material selection and shape design aspects. Surgical tools' specifications are case dependant. Usually the most used material is titanium for its light characteristics. Aluminum is used specially when reaching for tumors in a straight way manner. Up to date, the commonly used neuro-surgical tools have a lot of constraints in terms of flexibility and are a major factor in determining the surgery success — according to Dr. Bajwa, a neurosurgeon at Wilson's Hospital, NY. A tool known by the name of "*snake,*" Fig. 3, by similarity to its progressive motion is being developed but is restricted for small neurosurgical cases involving brain ventricles [24].

In this application, the ideal tool is one that will be progressing inside the brain layers in a "snake" fashion walk reaching for exactly the desired coordinates and avoiding vital cells and blood vessels. In order to minimize brain damage and avoid vital parts of the brain as the probe travels toward the tumor flexible, resistant, and allergic free materials are needed. It would consist of hollow concentric cylinders that extent under demand. A maximum deviation of 5° between two consecutive insertion depths of the surgical tool is allowed at this design. From the control unit, the surgeon or the robotic arm can execute the predefined plan. By a sensitive pressure mechanism the push buttons allow the tool to extend progressively in order to reach for the deep layers. The light gray refers to hollow cylinder allowing the sliding of the extensible parts. The pressure required to extend each part would be a function of the insertion depth. The extensible parts would have different strength depending on the insertion depth. By a rotation mechanism, the robotic arm or a surgeon can determine the angle of deviation wanted to achieve before the tip extends to reach the terminal point. Once the first strategic point is

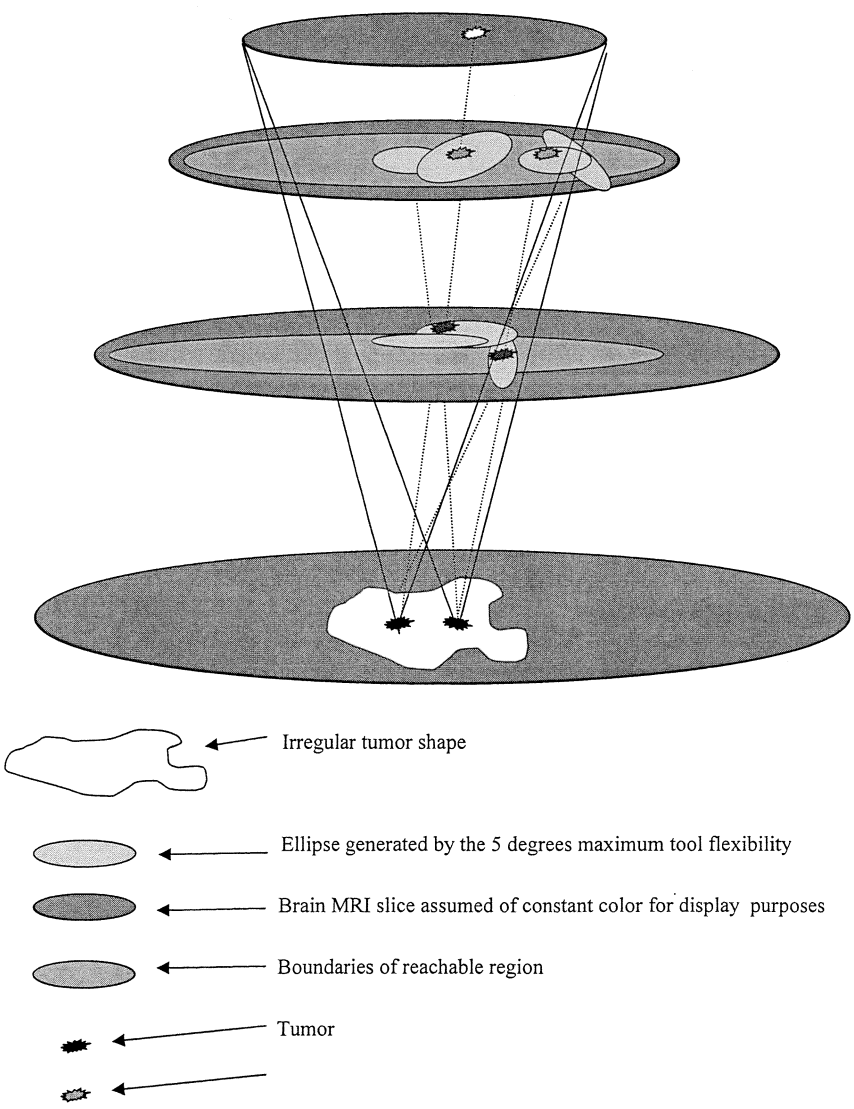

Fig. 9. Enclosed area for Approach B.

reached, two lateral extension would extend horizontally under a pressure mechanism for two reasons: 1) to lock the tool in this position and allow a precise extension of its tip, and 2) to make way for the tool tip into the brain layers.

The last tool extension that is extracting the tumor is a removable part that depends on the tumor type. For smoother insertion a V-point tip would be more suitable for the surgery specially that for deeply located tumor effort should be exerted on the brain cells to make way for an "intruder." When the surgical extensible tool's tip is a dull flat end, more damage and pressure is needed for insertion than in the case of a V-point.

This potential surgical tool would be feasible with the future micro-level technology that is changing our conception of instruments' size in a swifting revolutionary manner.

B. An Optimal Path Approach

The main purpose is to develop a "thinking algorithm," or strategy, for planning a surgery instead of the surgeon given some input from experts and many assumptions made by the author. The algorithm is intended to be a general case solver. The steps involved are:

1) From a set of 2-D MRI, volume representation using the marching cube theorem is performed.
2) Main goal is to reach a tumor with the least possible brain damage (if such a path exists) in an intelligent manner without irrelevant and redundant path calculation. The problem, at a first glance, is a NP type. Given a set of starting points on the cortex surface $\mathrm{S_s}$, a more or less straight path is desired in order to connect any point $\mathrm{P} \in \mathrm{S_s}$ to strategic point $\mathrm{C} \in \mathrm{A}$ where A is the set of infected brain cells that belong to the first infected slice T encountered in a surface to bottom penetration.
3) Once a path is identified, the information can be safely transferred to a slave robot in order to perform the extraction.

Decision-making is the key toward successful surgical operations. Even the most accurate surgeons are prone to errors and their performance, in similar surgeries, is alienated to their moods and their fatigue, which can drastically shape the outcome. The intra-operative MRI is a revolutionary achievement

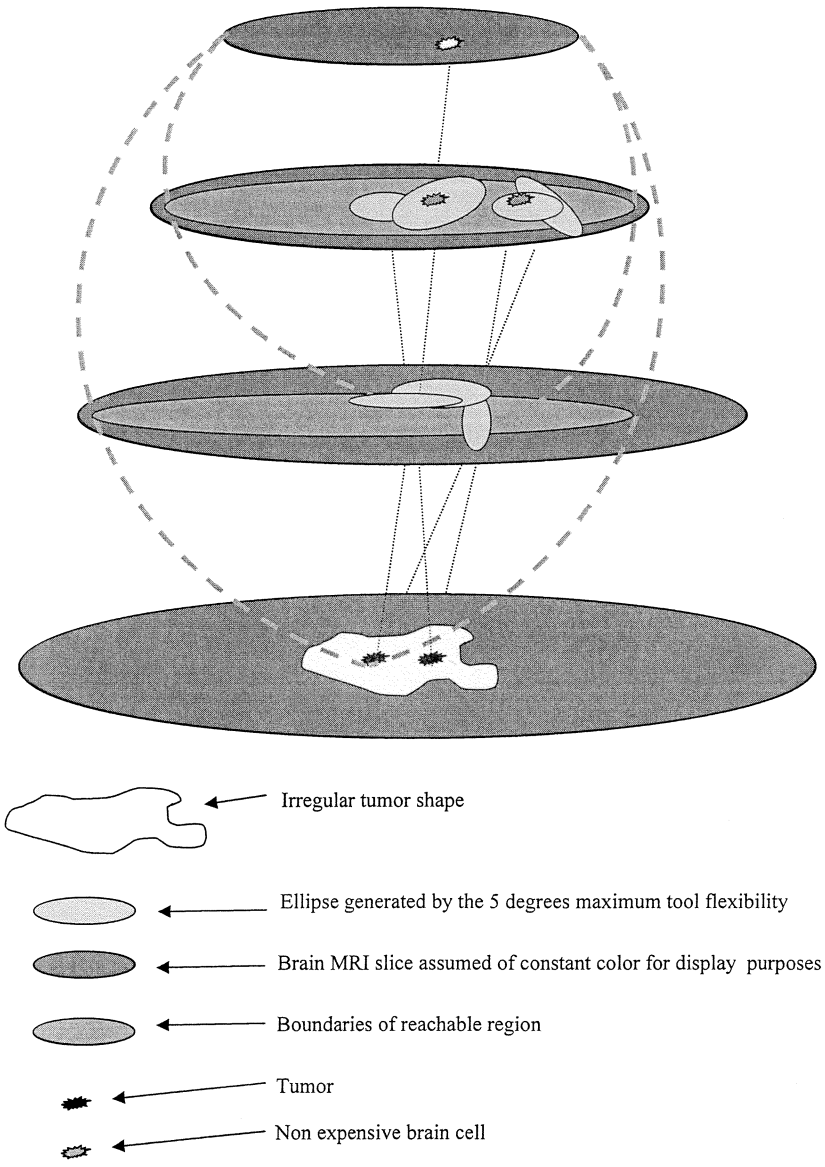

Fig. 10. Enclosed area for Approach C.

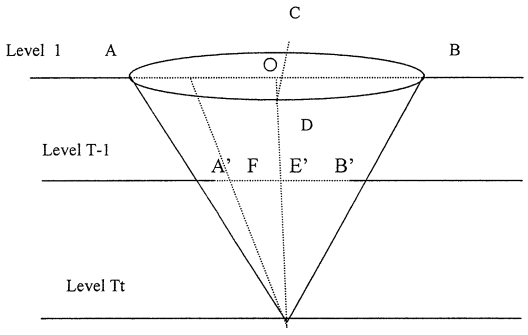

Fig. 11. Cone of paths in consecutive levels.

for surgery. The state of the art imaging technology, the quick data acquisition process, and the special set up of the operating room allow even more surgeons to take part in the decision-making thus reducing the potential risks of traditional surgeries. However the decision and the execution still stem from humans where experience, practice, subjectivity, and bias play an important role in decision-making. We believe that if the best surgical expertise's practice as well as today surgical tool's constraints were fed into a "smart" algorithm, the surgery will be moving toward safer milieu. Analyzing every case individually according to the expert state of the art approaches, the algorithm would return the optimal path to extract the tumor. This is an affordable approach for improving surgical outcome at no extra cost of surgical equipment and surgical room design. The application will be also useful for novice medical surgeons to test their plans versus the software outcome. This way the patient safety and recovery rate will not be affected to a great extent by the surgeon's personal experience and mood. We are not claiming that the robot surgeon using the available surgical tools in their present development can totally replace the human surgeon, and act independently, but if instructed efficiently and using Amsgtrom level surgical tools it can be a reliable slave to carry out the surgery with astonishing precision.

With its current implementation, this work doesn't take into consideration brain shift during the surgery, which is a serious

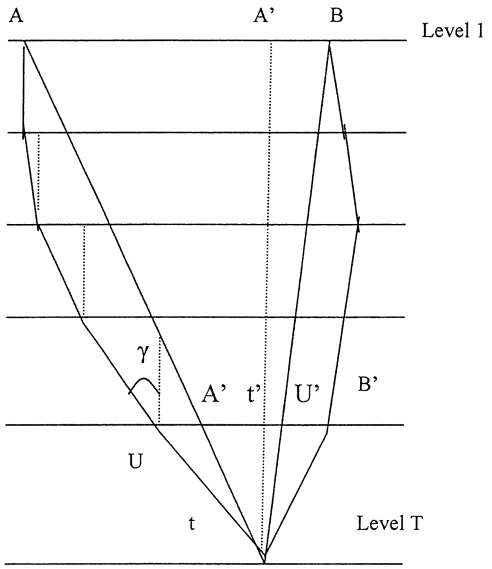

Fig. 12. Projected paths through consecutive layers.

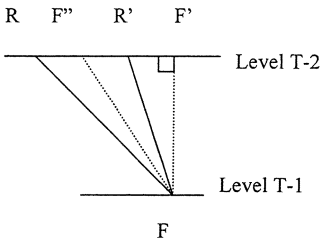

Fig. 13. Selection of the next point.

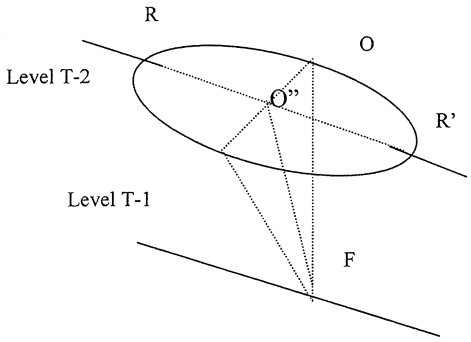

Fig. 14. Circular area within the same layer.

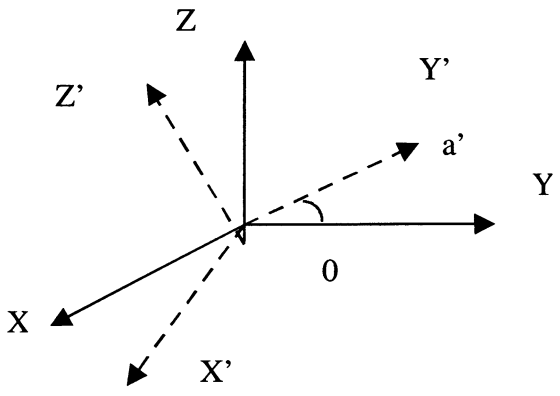

Fig. 15. The 3-D axis and the projected one.

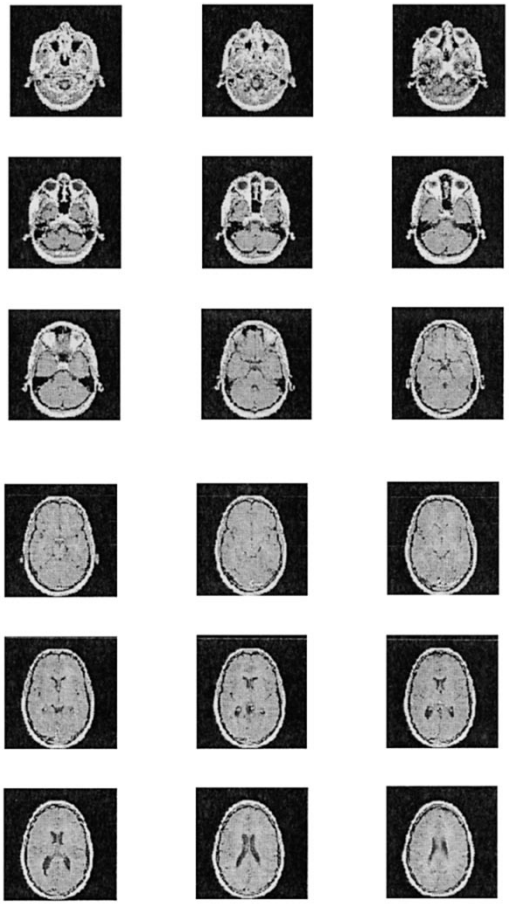

Fig. 16. Enhanced MRI set.

problem already raised in Section III. Future development of this work can focus on this aspect and the application will be more realistic.

C. Assumptions

In developing this approach, the following assumptions were made:

The tumor is a compact 3-D manifold. The search is applied to strategic points of the tumor. The surgical tool is constrained to a maximum degree of deviation from vertical position in penetrating two consecutive brain slices, its end's dimensions are of a pixel size. For a $256 \times 256 \times 128$ MRI stack, a total of 8.5 billions pixels can be displayed. Since the brain is estimated to have about ten billions cells, a pixel is 11 times a cell dimension. The tool flexibility function depends on the depth it has to travel inside the brain, the following relationship was used:

$$\vartheta = 0.0062\mathrm{n}^{\wedge 3} - 0.1574\mathrm{n}^{\wedge 2} + 0.8241\mathrm{n} + 3.8272$$

where n is the slice number and ϑ in degrees, Table I. For an assumed intra-planar distance of 13 mm:Once strategic tumor point $\mathrm{C} \in \mathrm{A}$ is reached via "the most appropriate path," the problem is solved. The MRI data set used in this application contains all the relevant anatomical and functional features necessary for practical surgical planning. The pixels are assigned integer values referring to the cells' functionality, their type and location with respect to vital areas, with the least expensive brain

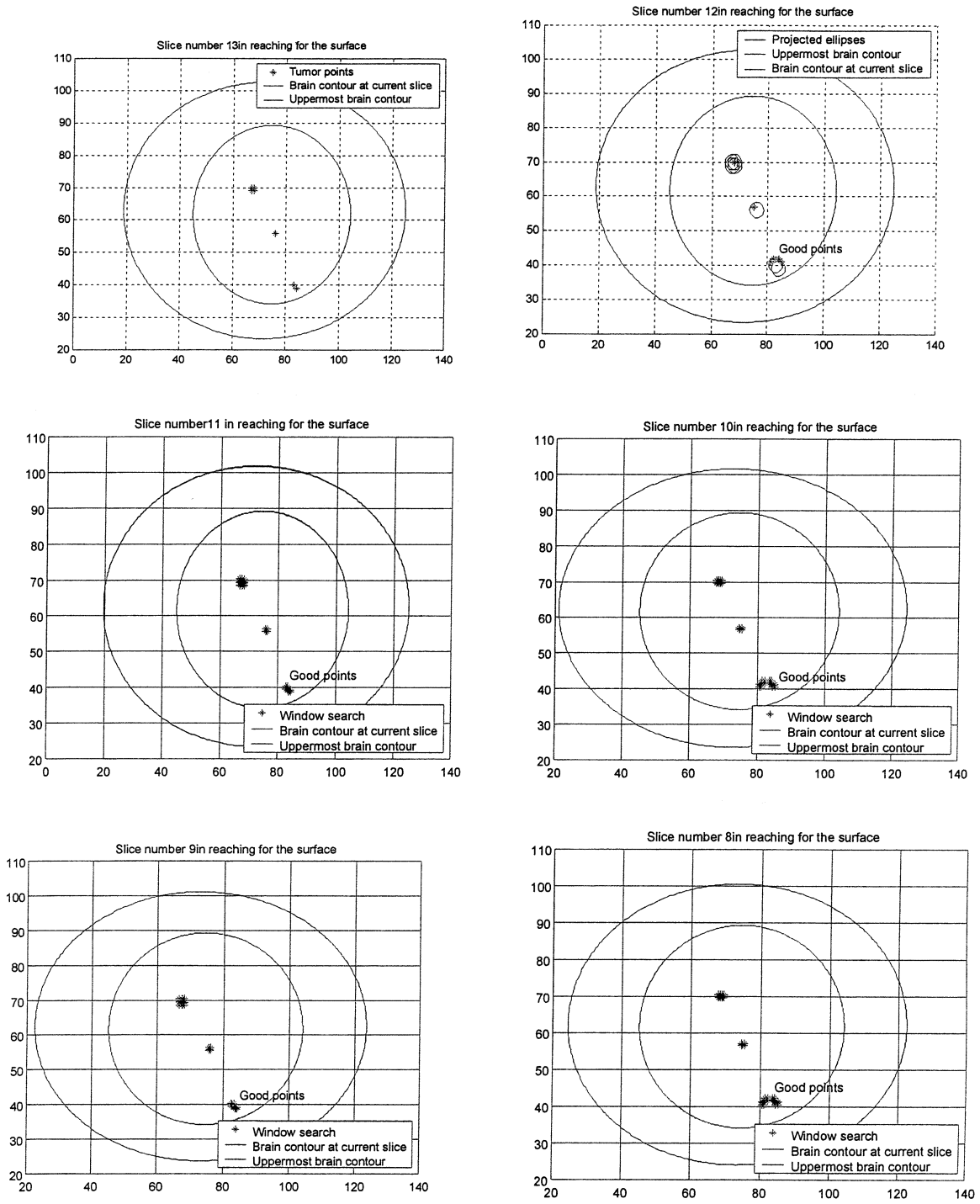

Fig. 17. Simulated results.

cells having the highest value. No brain shift modeling is taken into account, rather brain structures are assumed to remain in the same position preoperatively and during the surgery.

D. Methodology

The steps required for the modeling and implementation of the method proposed here are, Fig. 11–15.

1) Let S be a stack of N slices that cover the whole brain.

2) Every slice M of the stack S has an intensity matrix $\mathrm{I}(\mathrm{x},\mathrm{y},\mathrm{z})$ correlating every pixel to a scalar value. Every entry of matrix I is a function associating tissue type (which is obtained from the segmentation results of the MRI), to the functionality (obtained from the fMRI) to the tissue resistance, to the presence of the vessels within this point. We aim to minimize $\mathrm{I}(\mathrm{x},\mathrm{y},\mathrm{z})$ given the surgical tool constraints stated in the assumptions and that will be detailed in step 7.

—Let $\mathrm{Sen}(\mathrm{x},\mathrm{y},\mathrm{z})$ be a matrix representing functionality of the cells and their sensitivity with high values for important cells.

—Let $\mathrm{BL}(\mathrm{x},\mathrm{y},\mathrm{z})$ be a matrix representing presence of blood vessels with high values for arteries and primary veins.

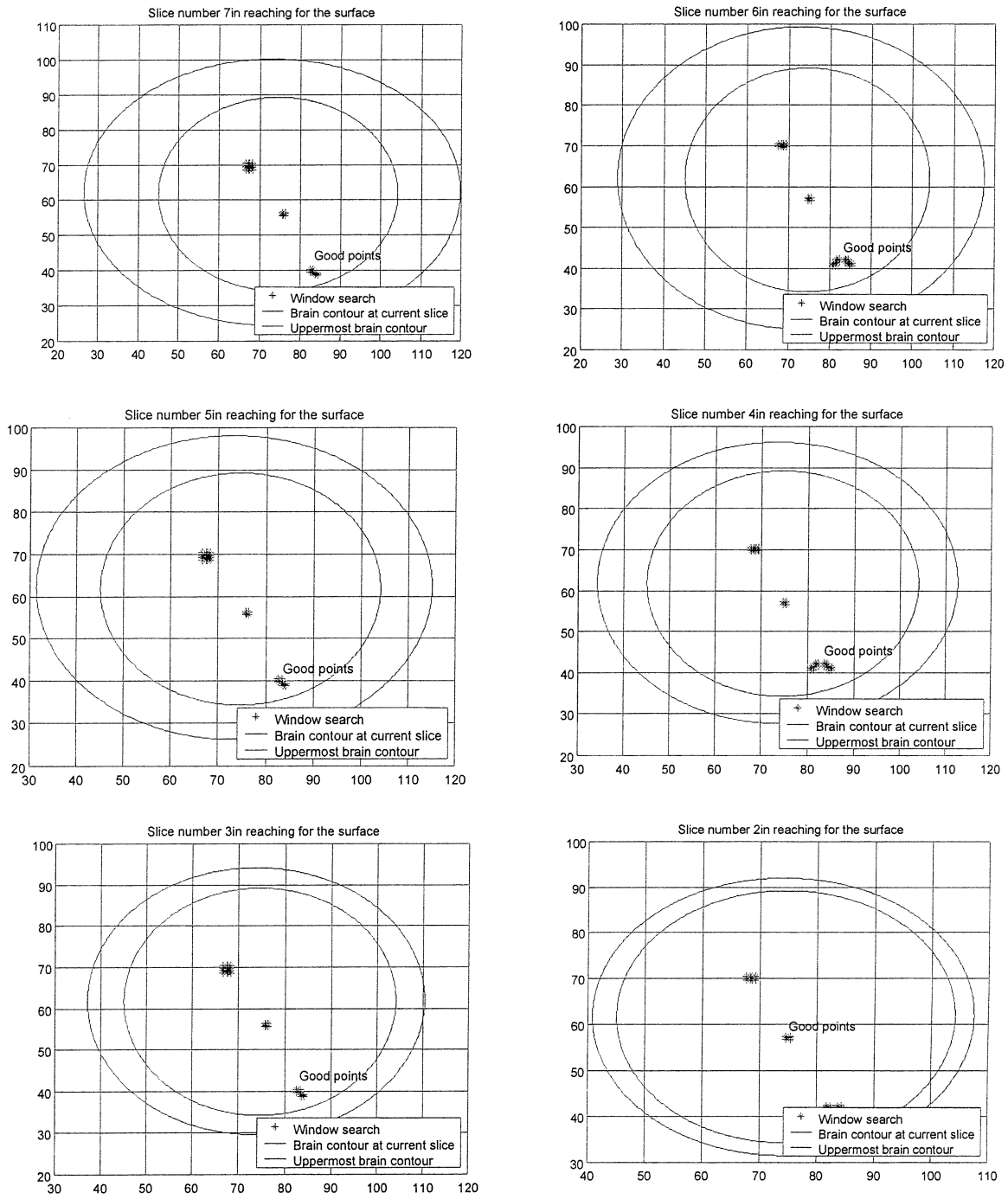

Fig. 18. Simulated results.

—Let $C_1(x,y,z) = \Pi Sen(x,y,z) * BL(x,y,z)$, so that brain cells with crucial functionality and high vascularity tend to have really high cost.

—Let $TI(x,y,z)$ be the tissue resistance of a given pixel.

—Let $F(x,y)$ be e^{-d} where d is the distance of point (x,y,z) from the center of gravity of the grouping of tissues it belongs to in this particular slice,

—$G(x,y) = F(x,y)/(F(x,y) + F(-x,-y))$ and

$$H(x,y) = G(-2d+2) \times G(2d+2)$$
$$C_2(x,y,z) = TI(x,y,z) \times z + H(x,y) \times TI(x,y,z)$$

—Finally $I(x,y,z)$ can be expressed as

$$I(x,y,z) = \Sigma C_1(x,y,z) + C_2(x,y,z)$$

TI, Sen, BL are determined by fMRI, MRA, and brain modeling characteristics they can be found in today's brain atlases. They are standard and patient independent.

3) Let $i = 1$ denotes the surface slice and $i = N$ the most bottom slice available in the Matlab MRI stack; see Fig. 4. It is actually a half set of MRI, covering till the eye and nose level.

4) Let $i = T$ denotes the first contaminated slice reached from the surface

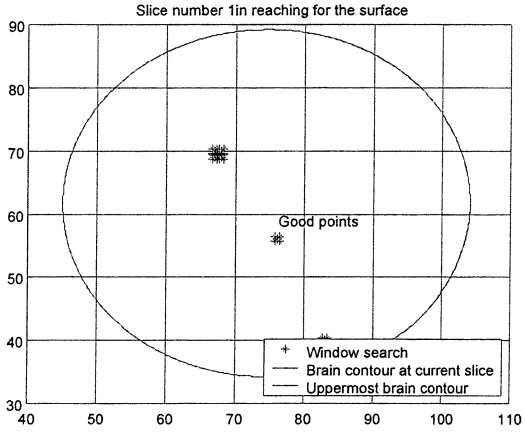

Fig. 19. Simulated results.

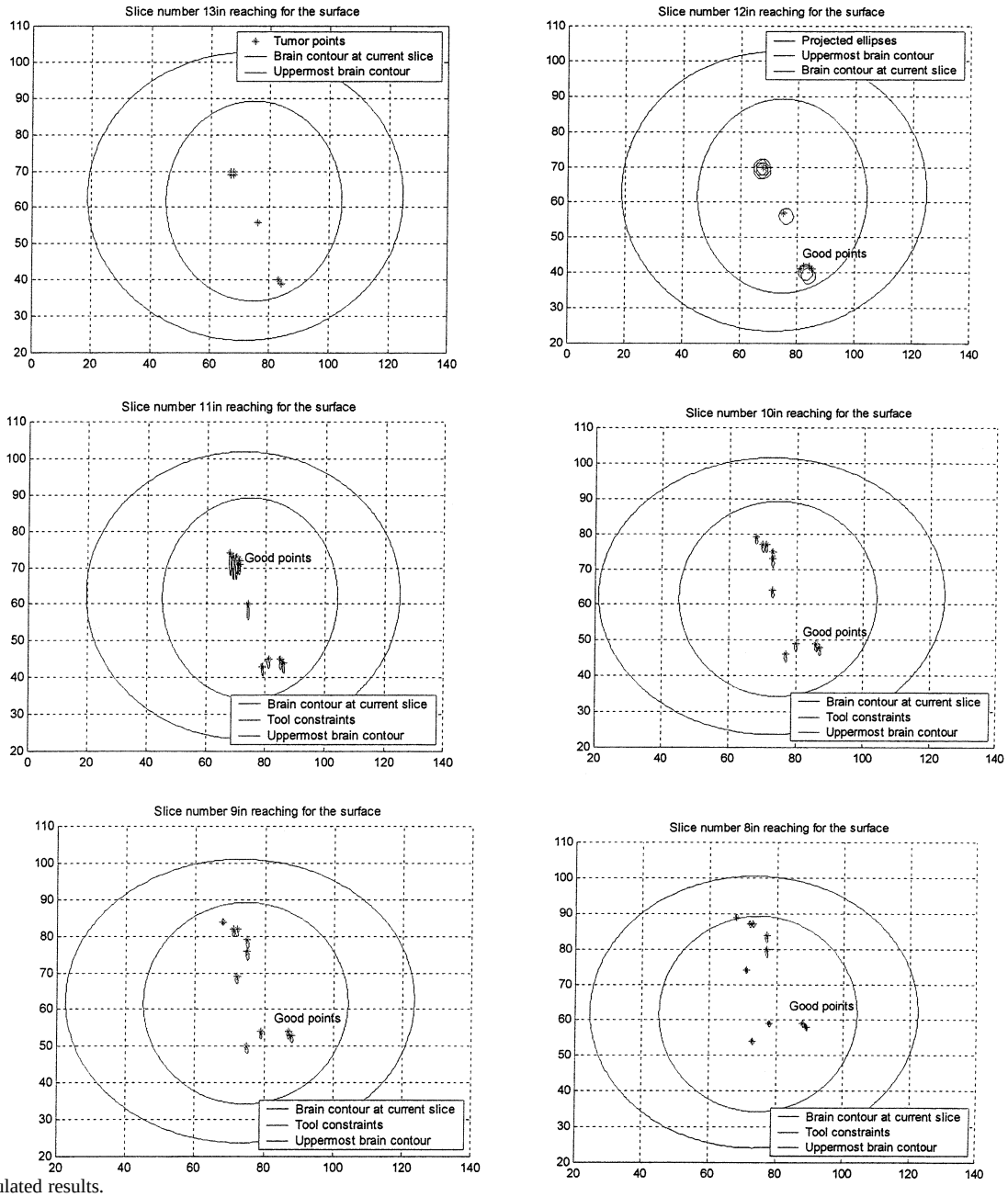

Fig. 20. Simulated results.

5) Let A be the set of all points corresponding to "ill" cells in slice T. We assume that A is a filled region with a continuous closed envelope. Tumor shape is case dependant and in most case unpredictable. In order to make the search smarter and less

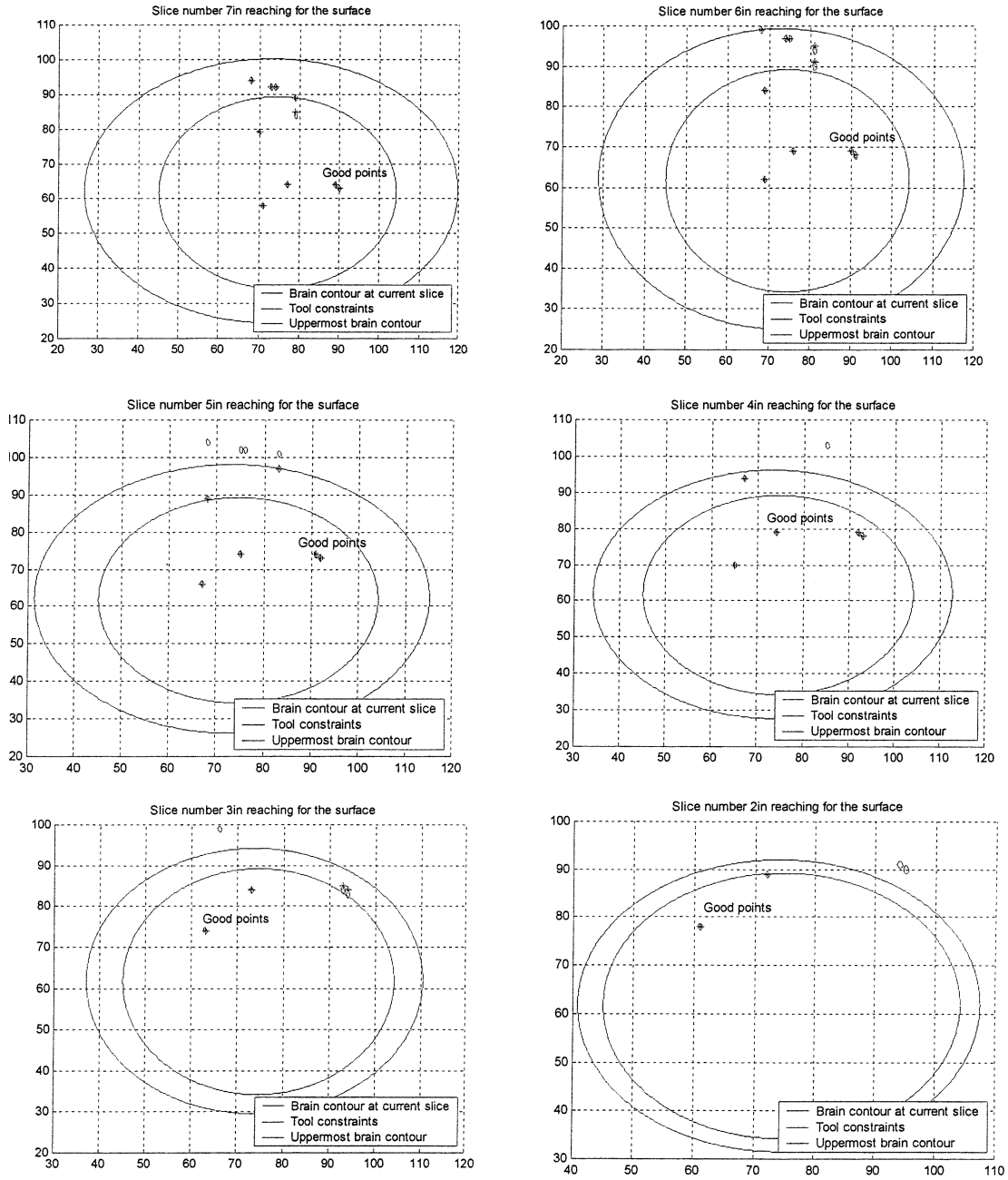

Fig. 21. Simulated results.

redundant, strategic points are assigned to some pixel values of area A. If A is a familiar geometric shape, the best points to retain for starting the search would be the center of gravity of area A as well as other centers of gravity for subareas created inside A. Fig. 4(d) illustrates some examples. If the tumor is an irregular shape -which is the practical case- edge detection followed by thinning algorithm and skeletonization procedures can be applied and the most essential line features of the tumor are retained. Along these representative lines mid-points (referred in Fig. 5 by black dots) are retained as strategic points

At this stage three different approaches were studied to solve this problem. The approach A (ordinary) assumes that the best path is confined to a vertical insertion and the tool is not allowed to have an initial angle with respect to the uppermost brain slice.

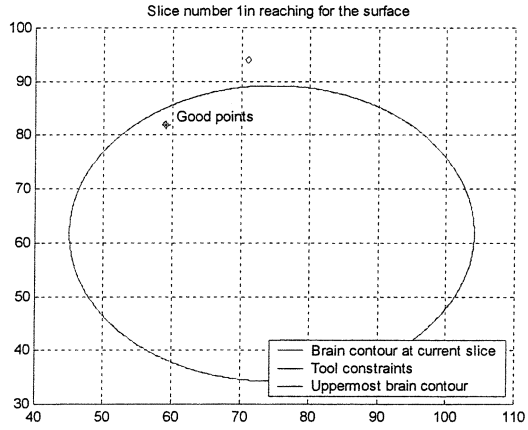

Fig. 22. Simulated results.

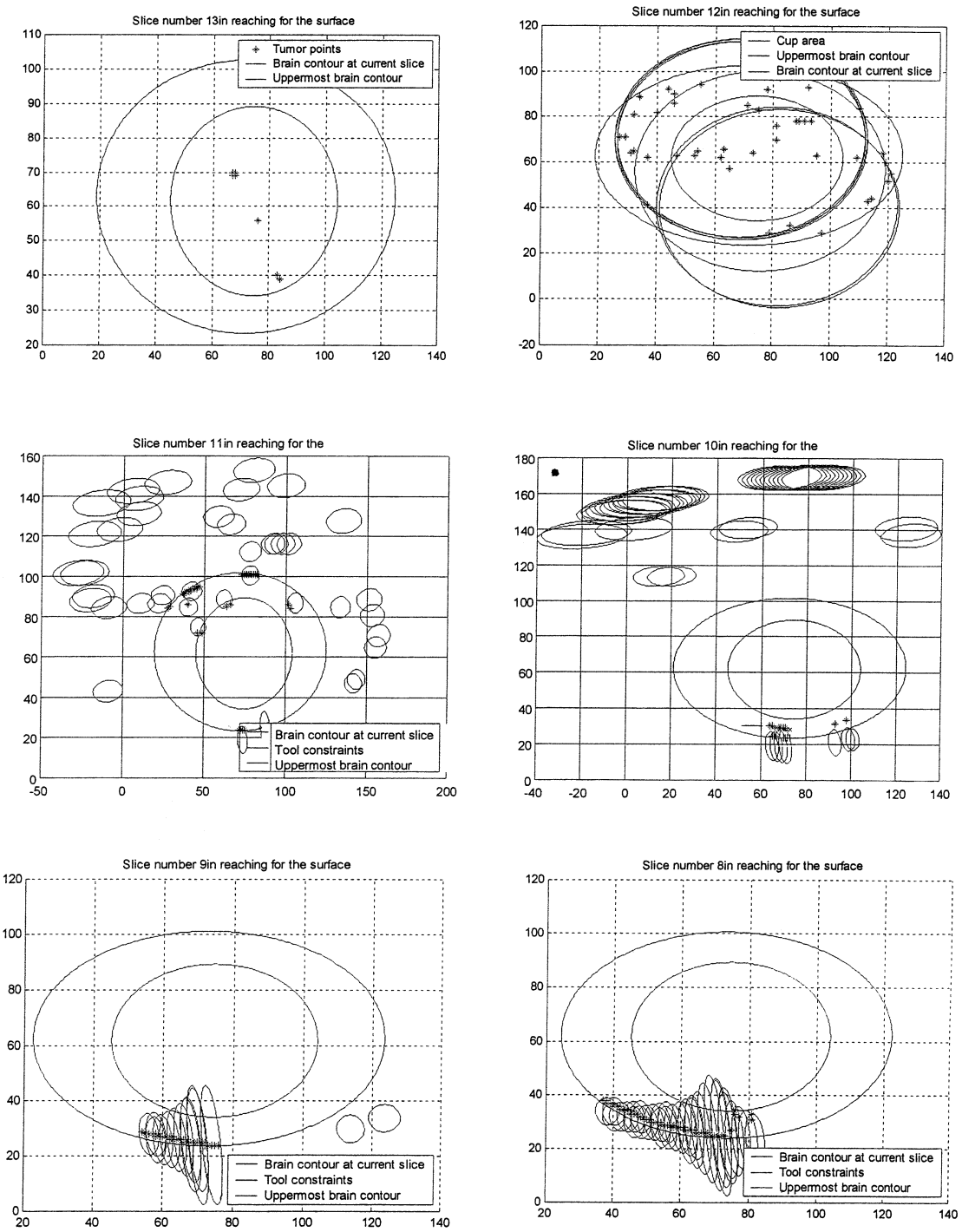

Fig. 23. Simulated results.

The search will include only pixels confined to a window built around the strategic tumor points and defined by the tool flexibility. An example is shown, Fig. 6, for illustration purposes. As can be easily guessed, this approach might not give the best possible path if this path exists along an angle with respect to the vertical.

Approaches B and C (Fig. 7–8) assume that the best path can have an angle with respect to the vertical. An ellipse E grouping all the physically possible starting points regardless of cost function and cells vitality is identified on the cortex surface on slice number 1 using a least square method (LSM) procedure. The center, minor Bm and major Am axis are calculated.

6) The physical possible starting space E is projected onto the subsequent slice of A. In this way we are able to track all the good subsequent points if the point $\mathrm{C}(\mathrm{x_j}, \mathrm{y_j})$ is the ultimate target of the surgical tool. This can be done using 2 approaches.

In the Approach B, ellipse E is projected on slice T-1 along the line joining one tumor pixel to the center of ellipse E, using simple geometry (Thales theorem). The search will be confined to the ellipse inside the conical shape in Fig. 9. This case is

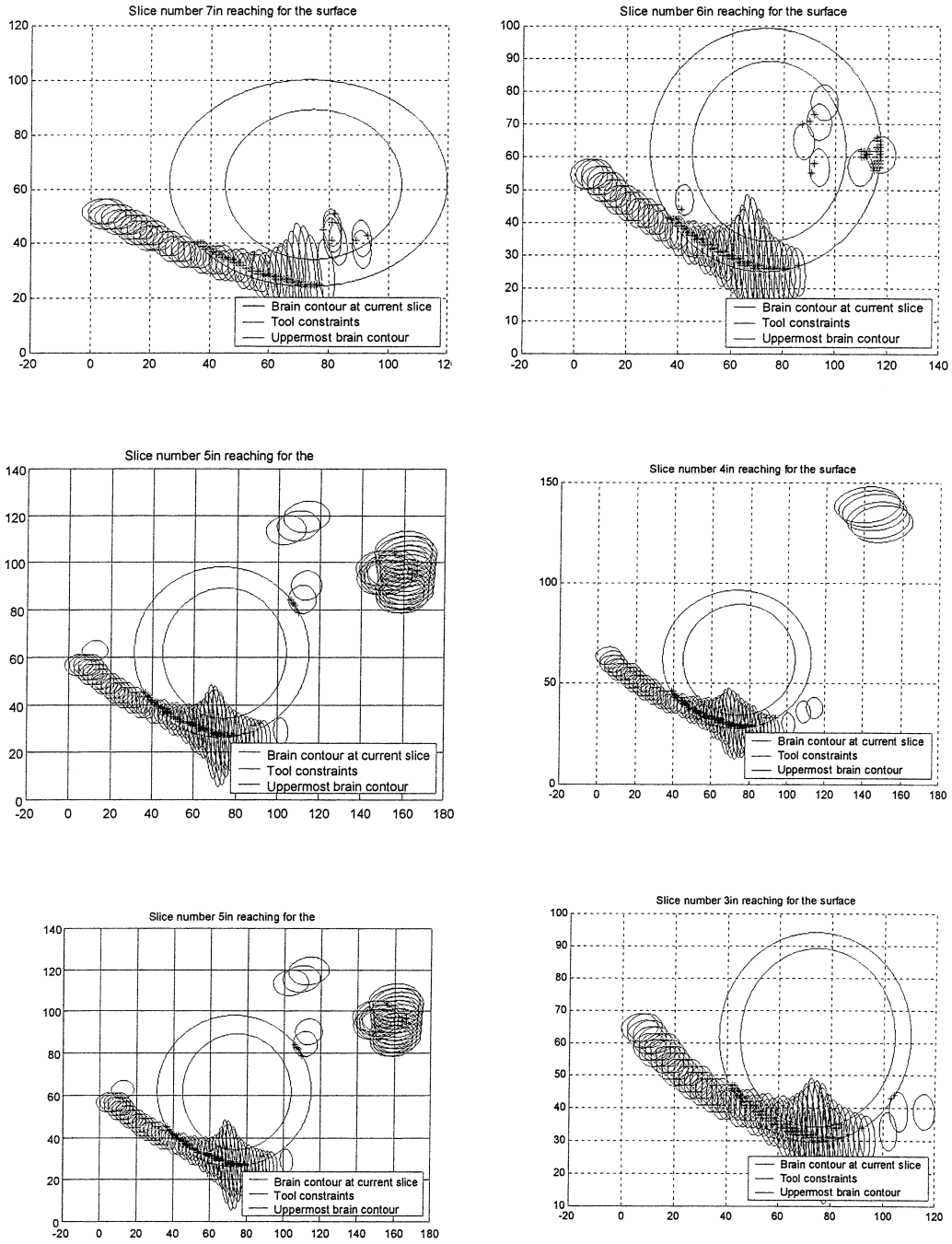

Fig. 24. Simulated results.

closer to most practical cases where the tool is really confined to straight path insertion. Studying the enclosed area by the cone and the brain contour at level T-1 will include all the possible straight paths targeting this particular tumor point.

In the Approach C the end points of the minor and major axis of the uppermost ellipse are joined to the strategic points of the tumor via a regular polygon whose angle and number of sides depend on the tool's flexibility as well the tumor's depth inside the brain. Notice that this approach gives wider intersections for subsequent levels of slice T than approach B, and it would probably return less expensive paths if these exist within the area not covered by approach B. The regular polygon will have an angle of: $(180^0 - (F-1)*alpha)/2$ where alpha is the tool flexibility, and F the current slice number.

7) The intersection of either method in 3-D space with the subsequent slice in a bottom to top manner is represented with a green ellipse $\mathrm{E1}$ in Figs 9–10. Evaluate $\mathrm{I(x,y,z)}$ for all the points within the region bounded by ellipse $\mathrm{E1}$ and the brain contour in slice T-1.

8) Let AT1 be the set of the nonexpensive pixels. Since the path decision cannot be made at this level, it is important to study all the pixels that can be good candidates and belong to the interval $[\min -\varepsilon, \min +\varepsilon]$. A path with absolute zero cost cannot be found, but a relatively inexpensive one is what we

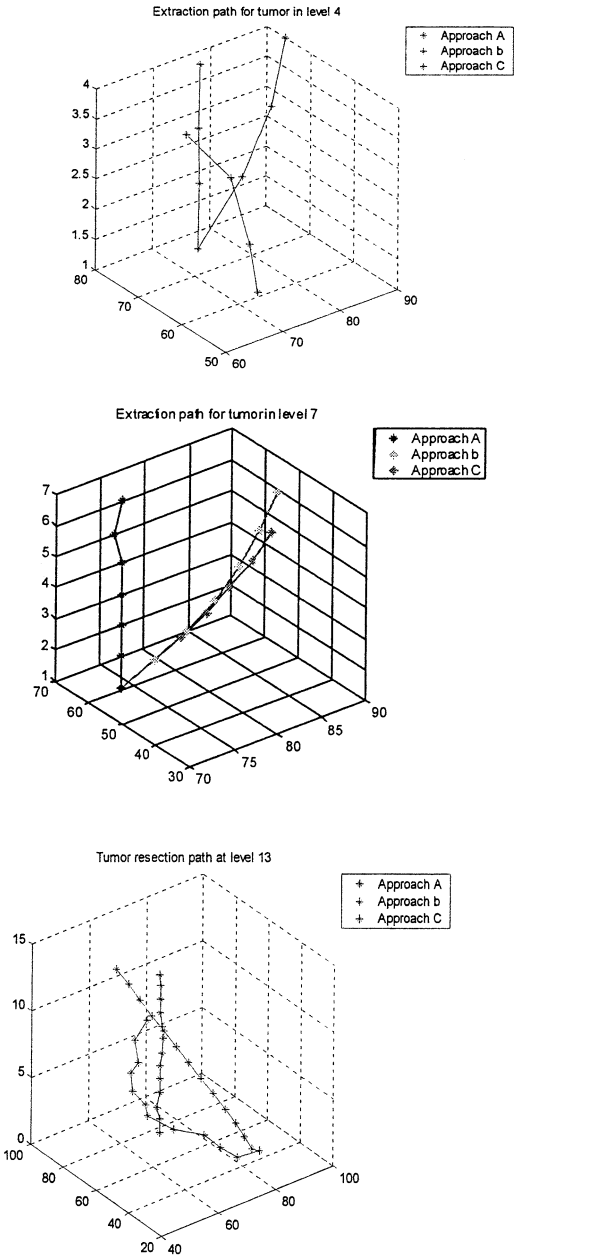

Fig. 25. Screening the candidate points retained at every level And searching for the least expensive reachable path.

are after ε is determined by assign a membership function to the pixel values in order to represent their degrees of "goodness." The membership function is a fuzzy one using the sigmoid function to restraint the search within acceptable limits. At every slice, the minimum cost MC to pay in order to go through this level is assumed known from the atlas discussed in step 2 and this value is mapped as 1 into the fuzzy set. While studying the pixel values enclosed by ellipse E1, elimination of expensive pixels is done according their "cost" with respect to MC. Grades are assigned to them and pixels that are within an acceptable range and that have at least one parent from the previous level are retained. All candidate points are stored and investigated because we are after the least expensive total cost of the path and rejecting at an early stage all points except one particular value will jeopardize the outcome and eliminate possible paths that starts rather high but end up real cheap. Since it might be common to have more than one good point that went through the preliminary selection in the same ellipse E1 that have more than one parent, it is important to keep track of the hierarchy of generation. Shades of grayness represent the fuzzy cost associated with the candidate points retained from every level.

9) From every point P of AT1, an ellipse EE is drawn on slice T-2 with major axis acc and minor axis bcc. The ellipse results from the intersection of slice T-2 with a cone having an opening of x degrees (x is a function of the slice depth) with respect to the line joining P and its parent pixel in slice T. These ellipses are represented in Fig. 1. Notice that "good children" pixels in level T-1 can have more than one parent in slice T. It is essential to keep track of the hierarchy of generation because the ellipses' directivities depends on it and the tool is constrained in its motion and cannot reach any point from anywhere.

10) The same procedure described above is applied for the "good children" pixels. They are projected along the line joining them to the parent pixel and the cone corresponding to the tool flexibility intersects the brain contour at slice T-2 resulting in an ellipse Ee shown in Fig. 1 that will enclose all the possible candidate pixels. Evaluate I(x, y, z) for only points. The least expensive points of cost CT2 are stored in AT2.

11) Step 8 is repeated until the brain cortex surface is reached. In order to determine the specific trajectory the tool has to follow, a backward search starts from the uppermost slice. The surface points that proved themselves good candidate are traced back and the total cost of the path is calculated. The least expensive path is chosen. It is not imperative that this path is not dangerous: it is the least expensive path to follow if an extraction is to be carried out. If many vital cells were involved, radio-surgery or chemical therapy would be safer in this case.

Appendix A: Given: Ellipse E enclosing brain contour at the uppermost level.

E has center O(xo, yo) with major axis OA = am, minor axis OB = bm.

Tumor t at level T.

Find the ellipse EE center, axis and orientation in level T-1;

OE is the cone axis of opening delta = arctan(OA/(T − 1) ∗ scaling) with scaling being the inter-planar distance between the MRI slices. E' is the vertical projection of tumor point E on plane T-1; Using simple geometry A'E' and E'B' can be found be

$$A'E' = \frac{\text{scaling}}{(T-1)*\text{scaling}} OA$$
$$\text{and } B'E' = \frac{\text{scaling}}{(T-1)*\text{scaling}} OB.$$

The major axis of ellipse EE is $am = (A'E' + B'E')/2$, and its minor axis $bm = (C'E' + D'E')/2$

If am > A'E' point E' has to be shifted to the left by an amount equal to (am − A'E') along the normalized vector A'E', otherwise E' is shifted to the right, and we obtain the true center of ellipse EE. Ellipse EE will have its major axis along the horizontal just like E.

Appendix B: We assume that tumor point t and the extremity A of the major axis of ellipse E are connected by a regular polygon with a number of sides equal to $n = 2 * pi/alpha$ so

TABLE II
SIMULATION RESULTS.

Tumor position	Computation Time	Number of enclosed points at T-1
in slice 13 @		
Approach A	173.89	
Approach B	40.75	143
Approach C	678.18	1302
in slice 10+		
Approach A	NA	
Approach B	27.41	117
Approach C	427.71	1164
in slice 7 *		
Approach A	192.08	
Approach B	30.65	269
Approach C	39.61	608
in slice 4 *		
Approach A	21.32	
Approach B	12.31	124
Approach C	30.7	548

*Tumor localized at (75,76); (74,61); (72,72); (68,70); (68,71); (69,70); (69,71); (67,68)

+ Tumor localized at (50,40);(50,41);(51,40);(51,41)

@ Tumor localized at (84,39);(83,40);(67,68);(69,70);(76,56)

the polygon angle is $\gamma = (PI - (T-1)\text{alpha})/2$; (alpha = tool flexibility angle).

Our purpose is to determine length UA'and U'B' in order to localize the intersection of the regular polygon in 3-D space with level T-1. The angle of the cone AtB is

$$\text{delta} = \arctan\frac{\text{A}''\text{A}}{(\text{T}-1)*\text{scaling}};$$

$\text{Ut}' = \text{scaling} * \tan(\text{delta} + \gamma)$.

Same procedure is applied with points (t, B), (t, C), (t, D) and the am1 major and bm1 minor axis length of the ellipse EE resulting from the intersection of the regular polygon in determined. The ellipse center will shifted from the projection of t on level T-1 with an amount equal to the difference between (am1-Ut') along the direction of vector tA.

Appendix C: Finding generated ellipse by tool constraints at level T-2 for both approaches B and C.

After analysis of ellipse EE (got from either approach B or C) pixel values, assume point F alone is retained as best candidate at this level. We need to draw the ellipse EEE corresponding to the tool constraints on level T-2. The axis of the cone which will intersects plane T-2 with EEE passes through points E and F. Let F" be the intersection point of this line with T-2 and F' the vertical projection of F on planeT-2

$$\begin{aligned}
\text{angle}(\text{F}''\text{FR}') &= \text{alpha} = \text{tool flexibility} \\
\text{F}''F' &= \text{scaling}*\tan(\text{F}''\text{FF}') \\
\text{RF}'' &= \text{scaling}*\tan(2*\text{F}''\text{FF}' + \text{R}'\text{FF}' \\
\text{R}'\text{F}' &= \text{scaling} * \tan\left(\frac{\arctan(\text{FF})}{\text{scaling}} - \text{F}''\text{FF}'\right) \\
\text{F}''\text{R}' &= \text{scaling} * \tan(\text{F}''\text{FF}') \\
\text{major axis of} & \\
\text{EEE am1} &= 0.5*(\text{F}''\text{R}' + \text{F}''\text{R}
\end{aligned}$$

TABLE III
SIMULATION RESULTS.

Tumor position	Comp. Time	Encl. pts	Cost
slice 13 @			
Approach A	40.75	40	857
Approach B	173.89	924	866
Approach C	678	3302	*979*
slice 7 *			
Approach A	12.08	60	536
Approach B	30.65	269	517
Approach C	39.61	608	*602*
slice 4 *			
Approach A	11.32	40	281
Approach B	22.31	592	315
Approach C	30.7	989	*319*

*Tumor localized at (75,76); (74,61); (72,72); (68,70); (68,71); (69,70); (69,71); (67,68)
@ Tumor localized at (84,39);(83,40);(67,68);(69,70); (76,56)
From the simulation, the higher the cost the better is the approach.

Center O" of EEE will be shifted from F" by an amount equal to (RF"-am1) along the normalized vector $\mathrm{F''F'}$ depending on the difference between RF" and am1.

The minor axis is perpendicular to the major axis. Using the dot product between vector FO" and RR' angle FO"Q is found. Using the sine rule in triangle FO"Q, O" Q can be found. Finally ellipse EEE translated to the origin rotated by the angle alpha $\acute{\alpha}$, then translated to its respective center using the following formulas for figure rotation:

$$\mathrm{X'} = \mathrm{X}{*}\cos(\acute{\alpha}) - \mathrm{Y}{*}\sin(\acute{\alpha}); \mathrm{Y'} = \mathrm{Y}{*}\cos(\acute{\alpha} + \mathrm{X}{*}\sin(\acute{\alpha}))$$

(Note that for axis rotation formulas are: $\mathrm{X'} = \mathrm{X}{*}\cos(\acute{\alpha}) + \mathrm{Y}{*}\sin(\acute{\alpha});; \mathrm{Y'} = \mathrm{Y}{*}\cos(\acute{\alpha}) - \mathrm{X}{*}\sin(\acute{\alpha})$

It is important to keep track of the parent that generate the good children at a subsequent level in order to be able to back track the path and not violate the tool constraint flexibility.

E. Simulation Results

The initial MRI set, Fig. 16, used is available in the Matlab 5.2 image processing toolbox. In order to improve the visual appearance of every slice T without modifying its pixel information, every pixel value is divided by the fraction $255/\max(\mathrm{T})$. The following MRI set results, Fig. 17–25, Tables II-III, from this enhancement operation

Matlab Simulation for a tumor assumed at level 13 and in the following positions (84,39); (83,40); (67,68); (69,70); (76,56); using approach A

Matlab Simulation for a tumor assumed at level 13 and in the following positions (84,39); (83,40); (67,68); (69,70); (76,56); using approach B

Matlab Simulation for a tumor assumed at level 13 and in the following positions (84,39);(83,40);(67,68);(69,70);(76,56);using approach C

An additional simulation was carried out for different tumor points, localized at different depth. Results for case studies are tabulated below.

From the simulation, the higher the cost the better is the approach.

V. CONCLUSION AND DISCUSSION

A. Discussion

Since the work was performed on a nonsegmented MRI set, there is no meaningful correlation between the anatomical brain differences and the pixel value. Total cost of the path is not relevant to favor one method over the other. Depending on a particular tumor's position, one approach would prove its supremacy over another. Since the patient safety is in question and there is no "free path" but rather cheap paths, it would be recommended to perform the three approaches and decide on the least expensive trajectory The three approaches cover all the possible ways to reach the tumor. Approach B is in a way a particular case of approach C. Ideally approach C is the best since it encloses more points to study at level T-1 thus there is more opportunities to pick cheaper paths than the other approaches. However, given the tool flexibility constraints, some cheap points at level T-1, might not lead to any good end, and approach C might not return the relatively cheaper path. In the following table, computations time as well as initial number of points investigated at level T-1 are tabulated. Time factor is really not the major concern because this analysis is done preoperatively and there is no time constraint. Besides given the ever-increasing speed of computers, processing and quick renderings are drastically improved.

B. Conclusion

Surgery planning and decision making are the key toward a successful operation.

With the image guided surgery, scans (MRI, CT, or PET scans) are acquired prior to surgery and loaded onto a computer workstation. The workstation is connected to a position sensor and the images registered to the patient just before surgery, or during surgery. The surgeon uses instruments connected to the position sensor to view the images at the location that he or she is touching. With all the state of the art imaging techniques and facilities, the surgeon has still to decide by himself or herself the way to resect the tumor.

If anatomical information as well as cells type, functionality and vessels position were coded in the MRI set and fed to an algorithm given the tool constraint that is intended to be, all the possible paths and their respective costs can be calculated. Since the algorithm will be choosing the path according to the experts rules and decision making, it would perform better than pure human decision where fatigue and personal problems will bias the surgeon decision and thus the outcome of the operation.

It will lead to smaller craniotomies, reduced hospital stays. It serves as a confirmation to surgeons in the case of tumors located in critical areas such as the motor cortex.

We tried to illustrate this by investigating all the possible paths that can reach the tumor given into consideration the tool flexibility constraints. Future work would perform the analysis on real segmented MRI data set, and would incorporate 3-D-path visualization with respect to brain anatomy. Modeling of brain shift has to be incorporated in order to make the application more realistic and helpful. With the sophisticated ultra sound features used in neuro-surgery, the path can be readjusted to accommodate for the brain shift.

REFERENCES

[1] "The National Institute of Neurological Disorders and Stroke's Guide Brain and Spinal Cord Tumors: Hope Through Research,", 1997–1999.

[2] *The American Brain Tumor Association's A Primer of Brain Tumors: A Patient's Reference Manual*, 1999.

[3] [Online]. Available: http://www.neurosurg.wayne.edu/gammaknife/gamma.html

[4] J. Loeffler and D. Shrieve, "Radiology," in The Brain Tumor Society's New Frontiers Symp., Boston, MA, Nov. 11, 1995.

[5] E. Profio, "Biomedical engineering," in *Radiology*. New York: Wiley, 1993, sec. 6, pp. 204–212.

[6] J. Ojemann *et al.*, "Functional MRI studies of word stem completion: Reliability across laboratories and comparison to blood flow imaging with PET," in *Human Brain Mapping*. New York: Wiley, 1998, vol. 6, pp. 203–215.

[7] [Online]. Available: www.uke.uni-hamburg.de/Institutes/IMDM/IDV/Articles/cga92po/

[8] [Online]. Available: http://splweb.bwh.harvard.edu:8000/pages/papers/ieee_95/ieee.gif

[9] [Online]. Available: http://www.tbts.org/mono/btmtoc.htm

[10] [Online]. Available: http://www.ai.mit.edu/projects/vision-surgery/surgery_home_page.html

[11] D. L. G. Hill, C. R. Maurer, R. J. Maciunas, J. A. Barwise, J. M. Fitzpatrick, and M. Y. Wang, "Measurement of intra-operative brain surface deformation under a craniotomy," *Neurosurgery*, vol. 43, pp. 514–528, 1998.

[12] M. Audette and T. M. Peters, *Algorithmic Overview Surface Reg. Tech. Med. Imaging Medical Image Process.*, vol. 1998.

[13] G. Berger, P. Rosch, and L. Steffgen, *3-D Rrecon. Intracranial Vessels Using Color Doppler Energy Method Initial Experiences Ultraschall Med.*, vol. 17, pp. 277–280, 1996.

[14] A. Gronningsaeter, G. Unsgard, S. Ommedal, and B. A. Angelsen, *Ultrasound-Guided Neuros.*, vol. 10, pp. 161–168, 1996.

[15] [Online]. Available: http://www.calix.com/nasamail/May_1996/mgs00115.html

[16] [Online]. Available: http://web.mit.edu/newsornce/nr/1998/lemerson.htm

[17] [Online]. Available: http://splweb.bwh.harvard.edu:8000/pages/papers/image.guided.surg2/index.html

[18] *The World Book Encyclopedia* , 1995 ed., pp. 561–570.

[19] B. Diallo *et al.*, "Voxeline: A software program for 3-D real time visualization of biomedical images," *Comput. Med. Imaging Graph.*, vol. 22, pp. 275–289, 1998.

[20] [Online]. Available: http://www.mhri.edu.au/~pub/modeling/cortex/cortex2.html

[21] W Schroeder *et al.*, *The Visualization Toolkit, An Object Oriented Approach to 3-D Graphics*, 2nd ed. Englewood Cliffs, NJ: Prentice-Hall.

[22] N. Bourbakis, D. Kavraki, and A. Mogzadeh, "Synpaper of MRI images producing 3-D shapes by request," in *Proc. SPIE Woskshop Visual Data Exploration Analysis*, vol. 2410, CA, Feb. 1995, pp. 432–437.

[23] M. Awad, "A Robotic Based Neurosurgery Using MRI Images," M.S. thesis, Boston University, Boston, MA, 1999.

[24] M. Awad and N. Bourbakis, "A robotic based surgery using 3-D MRI images," in *Proc. IEEE Symp. IAR*, 1999, pp. 126–132.

[25] A. King *et al.*, "Recent advances in biomechanics of brain injury research review," *J. Neuro.*, vol. 12, no. 4, pp. 651–658, 1995.

[26] S. Atkins, "Fully automatic segmentation of the brain in MR," *IEEE Trans. Med. Imag.*, vol. 17, Feb 1998.

[27] M. Clark *et al.*, "Automatic tumor segmentation using knowledge-based techniques," *IEEE Trans. Med. Imag.*, vol. 17, Apr. 1998.

[28] D. Roberts *et al.*, "Intraoperative brain shift and deformation: A quantitative clinical analysis of cortical displacements in 28 cases," *Neuro. J.*, vol. 43, no. 4, pp. 749–760, 1998.

Nikolaos G. Bourbakis (F'96) received the B.S. degree in mathematics from the National University of Athens, Athens, Greece, and the Ph.D. degree in computer science and computer engineering, Department of Computer Engineering and Informatics, University of Patras, Patras, Greece, in 1983.

He is currently a Distinguished Professor in CSE and the Director of the Information Technology Research Institute (ITRI) at Wright State University, Dayton, OH. Previous academic positions have included Associate Director of the Center on Intelligent Systems, Director of the Image-Video-Vision and Applied AI Research Lab., Professor of electrical engineering with joint appointment to the Computer Science Department at State University of Binghamton, Binghamton, NY, Professor and Lab Director at Technical University of Crete, Greece, Senior Scientist at IBM, San Jose, CA, and Assistant Professor at George Mason University, Fairfax, VA. His industrial experience includes service to IBM and Soft Sight, Binghamton.

Dr. Bourbakis is the Founder and Vice President of the AIIS, Inc., Binghamton, NY. He pursues research in applied AI, machine vision, bioinformatics/bioengineering, information security, and parallel/distributed processing funded by USA and European government and industry. He has published more than 230 articles in refereed International Journals, book-chapters and Conference Proceedings, and ten books as an author, coauthor or editor. He has graduated 11 Ph.D. and 30 Masters students. He is the founder and the EIC of the *International Journal on AI Tools*, the Editor-in-Charge of a *Research Series of Books in AI* (WS Publisher), the Editor-in-Charge of a *Research Series of Books in Bioinformatics* (upcoming, KAP Publisher), the Founder and General Chair of several International IEEE Computer Society Conferences, Symposia and Workshops (*Tools with AI, Intelligence in Neural and Biological Systems, Intelligence, Image, Speech and Natural Language Systems, Information and Systems, Bioinformatics and Bioengineering*, etc.). He is or was an Associate Editor in IEEE KNOWLEDGE AND, DATA ENGINEERING, and in international journals (*EAAI, PRAI, PR, PAA, ISR, COIS*, etc.,) and a Guest Editor in 14 special issues in IEEE and international journals related to his research interests. He is a Distinguished IEEE Computer Society Speaker, an NSF University Research Programs Evaluator, an IEEE Computer Society Golden Core Member, an External Evaluator in University Promotion Committees, an Official Nominator of the National Academy of Achievements for Computer Science Programs, and a keynote speaker in several International Conferences. He is also listed in many organizations (*Who's Who in Engineering, in Science, in Education, in Intellectuals, in Computer Engineering, AMWS, List of Distinguished Editor*s, etc.). His research work has been internationally recognized and has won several prestigious awards. Some of them are IBM Author recognition Award 1991, IEEE Computer Society Outstanding Contribution Award 1992, IEEE Outstanding Paper Award ATC 1994, IEEE Computer Society Technical Research Achievement Award 1998, IEEE I&S Outstanding Leadership Award 1998, IEEE ICTAI 10 years Research Contribution Award 1999.

M. Awad received the B.S. degree from Lebanon, American College, the M.S. degree in computer engineering with medical applications from the State University of New York, Stony Brook, in 1999. She is pursuing the Ph.D. degree from Unversity of Vermont, Burlington.

Ms. Awad is currently with IBM, VT.